Proceedings of the ASME 2023
International Design Engineering Technical Conferences & Computers and Information in Engineering Conference
IDETC-CIE 2023
August 20–23, 2023, Boston, MA

DETC2023-114893

EFFECTS OF RECYCLED PERMANENT MAGNETS ON ELECTRIC MACHINE AND HYBRID ELECTRIC VEHICLE PERFORMANCES

Saulius Pakštys[1,*], Angelo Bonfitto[1], Shailesh Hegde[1], Gaizka Ugalde[2], Fernando Garramiola[2], Christian A. Rivera[2]

[1]Politecnico di Torino, Turin, Italy 10129
[2]Mondragon Unibertsitatea, Mondragon, Spain 20500

ABSTRACT

Permanent magnet price volatility is an ongoing issue that affects many industrial sectors worldwide, dictating the costs of the final product by a substantial degree. This fluctuation can be attributed to a large concentration of NdFeB magnet production and material sourcing occurring in concentrated geopolitical areas, thus motivating institutions and governments to look elsewhere for magnet material for various applications. The work presented in this paper aims to determine the viability of recycled permanent magnets in electric machines used within the automotive industry. Magnet recycling incentives are presented, along with the two main routes for magnet reprocessing. They are briefly compared to present the route selected within this study. The recycled magnets used in this study are characterised such that relevant parameters are extracted for further analyses. A P2 hybrid electric vehicle is modelled and its energy management system presented, being an Equivalent Consumption Minimisation Strategy. The performance evaluation of a baseline machine at component level is performed, with its affect on vehicle performance quantified, followed by the recycled magnet machine's characterisation and subsequent performance evaluation at vehicle level. The recycled magnets inhibit a minor efficiency degradation at component level, leading to a performance degradation of about 0.11% at vehicle level.

Keywords: Emissions, Energy storage systems, Environmental, FE-Simulations

1. INTRODUCTION

The current status of climate change is of prominent concern to governments, institutions and industries worldwide. The automotive industry plays a large role in contributing to the production of greenhouse gases (GHG), thus compelling lawmakers to impose stricter thresholds on vehicle manufacturers regarding CO_2 emissions. Currently, hybrid electric vehicles (HEVs) and electric vehicles (EVs) offer the benefits of reducing these emissions substantially. The latter has gained significant traction in the market over the past few years, however has a particular shortcoming. Given that public charging stations are not as ubiquitous as gas stations, HEVs and plug-in hybrid electric vehicles (PHEVs) can solve the problem of range anxiety for consumers, while still maintaining environmental impact goals set by legislators. For instance, the European Commission has put in force a set of CO_2 emission target values for the year 2020 onwards [1] for cars and vans. A penalty of 95 euros per CO_2/km will be incurred to automakers if the average of the manufacturer's fleet exceeds the set target levels, thus emphasizing an economic incentive for the electrification of vehicles in addition to an environmental one.

With the inclusion of an increasing number of electric and electronic components on board comes the need for particular materials, ones that are typically concentrated in select geopolitical regions of the globe. One of these components are lithium-ion batteries which require lithium that is majorly concentrated in South America, China and the United States of America (USA) [2]. Other components such as permanent magnet synchronous machines (PMSMs) used for propulsion require rare earth elements (REEs) for the neodymium-iron-boron (NdFeB) magnets they contain. These elements have been identified to have a large concentration in South America (Brazil) and the Asia-Pacific region (China) [3]. Due to their increasing demand, nations have the liberty to use REEs as a powerful tool in trade wars against other countries, with China using them against the USA in 2019 for instance. In addition, as the demand increases for these materials, so will the electronic waste as EVs and HEVs reach their end-of-life (EOL), motivating the need for recycling strategies for the various materials present. A comprehensive literature review on battery recycling [4] indicates the various EOL battery recycling methods and their recovery efficiency of valuable metals. Due to the high cost of lithium, battery costs can be greatly controlled through recycling and in turn the price

*Corresponding author: saulius.pakstys@polito.it.

of the electrified vehicle, whether it is an EV or a HEV. The same can be done with NdFeB magnet recycling due to their high in-use concentration and economic value, with studies in their recycling from various sectors including the automotive industry indicating great potential, however also shortcomings [5–7]. It has been shown that re-sintered magnets consume 88% less energy in production with respect to primary manufactured magnets [8], suggesting an insight to this potential. However, limitations do exist and typically depend on the recycling route adopted, whether it is direct or indirect. The authors in this paper have however, identified a need to examine the direct impact recycled materials have on vehicle performance along with component level impact given the minimal amount of studies having been performed thus far.

HEVs can be classed into categories based on the position or size of the electric power source. Considering size, hybrid layouts are classed into micro, mild, full and plug-in types, with electric-only propulsion possible for the latter two types [9]. The following work focuses on a parallel full HEV as a case study, with a P2 configuration. The vehicle is of a light duty commercial (LCV) type. The aim is to study the effect of recycled permanent magnets on the performance of the electric machine (EM) and of the vehicle. This is evaluated through the performance comparison of the recycled magnet (RM) EM with that of the virgin magnet (VM) EM. The evaluation is then extended to the vehicle level, where it is evaluated in unloaded and loaded conditions.

The paper is organised as follows: first an introduction into the recycling potential of magnet material is presented, followed by the magnet characterisation and EM modelling. Subsequently, the vehicle model is discussed along with its control strategy and finally the simulation results are presented and analysed.

1.1 Magnet recycling incentives

A brief overview of the current recycling status of NdFeB material as well as the core reasons for its recycling must be addressed to justify the following work. Neodymium-iron-boron (NdFeB) magnets are, as of yet, the best performing magnets due to their high energy product (BH), thus making them suitable for traction drives in EVs and HEVs. In addition, EMs manufactured with these magnets display smaller sizes when compared to EMs outfitted with ferrite magnets, as well as a lower environmental impact [10]. NdFeB magnets are produced from a combination of various rare earth elements (REEs) such as neodymium (Nd), praseodymium (Pr), dysprosium (Dy) and terbium (Tb). Dy for instance is crucial for the automotive industry as it increases the thermal resistance of the magnet, therefore allowing the machine to operate at high temperatures. However, given the high cost of these elements such as Nd and Dy, 70% of the EM cost is attributed to that of the magnets [11].

As of 2020, less than 1% of REEs are recycled due to various drawbacks such as inefficient collection and technological difficulties [12]. Particularly, this can be due to the consequence of magnet recycling, where hazardous components are removed a-priori (such as screens and batteries) and the remaining electronic components are shredded. Subsequently, the concentration of NdFeB material is low and it is difficult to increase its concentration in a profitable manner. A study has shown [13] that the primary supply of REEs will be unable to meet demand scenarios by 2050. The same work suggests that a secondary supply from recycling can meet almost 50% of long term demand, around 2100.

Another incentive for tapping into discarded NdFeB material is economic. A technical report [14] indicates that China produces 97% of the total world production of rare earth oxides (REOs), while 75-80% of NdFeB production occurs there as well. In comparison, Japan is responsible for 17-25% while Europe accounts for 3-5%. China's control of the REE market induces large price variations that cause severe impacts towards companies that rely or supply these elements [15]. With such a polarisation in material processing, there is a considerable interest in decreasing reliability on one nation that can dictate the price fluctuation of the material, as well as decreasing environmental impacts. Projects such as RECVAL and DEMETER have been initiated with the aim to develop recycling strategies for EOL magnet material coming from industrial, consumer and automotive products [16, 17].

Currently, two main routes exist for magnet recycling: direct and indirect. The former considers reprocessing magnets into new magnets while the latter is concerned with chemical decomposition of discarded magnets into their fundamental REEs. Of the two, direct recycling, in which hydrogen decrepitation and complete magnet re-use fall into, is more energy and chemically efficient, and thus is the preferred method of choice. Hydrogen decrepitation uses hydrogen to crush the EOL magnets into a powder that is then pressed and sintered into new magnets. A study has shown [18] this process is promising for the extraction of NdFeB material from hard disk drives, and can be extended to automotive scrap rotors [6]. However, it does pose its own limitations, where the recycled powder contains a greater carbon content due to the binding materials present within components such as rotors of EOL EMs. Furthermore, re-sintered NdFeB material contains 2000-5000 ppm oxygen, while in comparison primary cast NdFeB contains 300-400 ppm [10]. With this in mind, it can be reasonably hypothesised that regenerated magnets will exhibit poorer performance characteristics when compared to their virgin counterparts. In fact, a study [19] has shown that due to the oxygen presence, the grain boundary (GB) phase does not melt any longer due to the higher melting point of the oxide, and therefore full magnet density cannot be achieved. Therefore the GB phase must be replaced, whereby the remanent flux density decreases by 2-10%. Considering the recycling of magnets from EMs, currently a unified recycling process has not yet been developed due to the various machine topologies present.

2. RECYCLED MAGNET CHARACTERISATION

The EM virgin magnets are standard commercial N42UH sintered NdFeB magnets with a mean remanence value of 1.30 T at a room temperature of 20°C with a relative permeability of

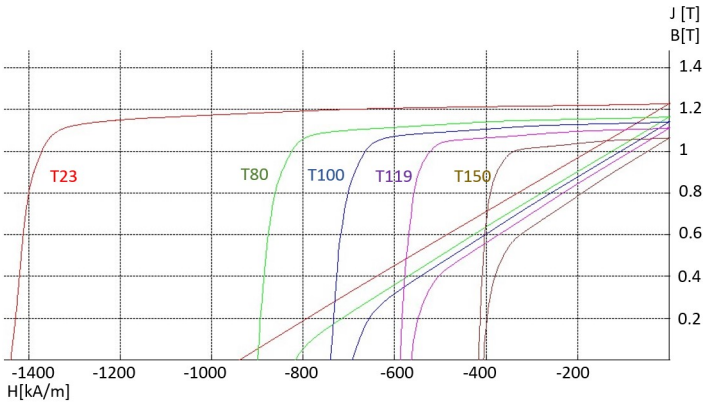

FIGURE 1: RECYCLED MAGNET B-H CURVE

1.052. The recycled magnets on the other hand are produced from 60% of recycled magnet powder and 40% virgin magnet powder. The recycled powder is created from EOL magnets using hydrogen decrepitation. This composition was reached on the basis of trial characterisations of varying portions of virgin and recycled magnet powder. Particularly, the best compromise of magnet characteristics and amount of recycled material is reached through the ratio selected. The recycled NdFeB magnet has a relative permeability of 1.041 and 5.2% lower remanence at room temperature than its virgin counterpart. Figure 1 shows the measurements taken in Mondragon Unibertsitatea's facilities of the recycled magnet samples at different temperatures. The names of the curves directly correspond to their associated temperature. The data pertaining to these curves is collected in Tab. 1.

3. ELECTRIC MACHINE CHARACTERISATION

This section shows the machine's efficiency map for both cases, virgin, and recycled magnets. The EM is an interior PMSM consisting of thirty slots and ten poles pair. First, the motor is modeled through finite element analysis on Altair® Flux2D and validated with standard N42UH sintered NdFeB magnets (representing the virgin magnets). Once the model validation is complete, the magnets are substituted with the developed recycled magnets shown in Section 2, taking into consideration the data at different temperatures.

Figure 2 displays the EM performance for the virgin magnets. The plot shows two regions of operation. The continuous duty cycle (S1) and peak region. The S1 curve is the dashed line starting at 150 Nm. All operating points on and below this curve consider a continuous operation magnet temperature limit of 110°C. In other words, the plot's efficiency values obtained on and below this curve cannot surpass a magnet temperature of 110°C in continuous operation. The peak operating points are those above the S1 curve and contemplate a fixed magnet temperature of 110°C. The reason is that these points are considered temporal and never continuous. Figure 3 shows the temperature regions of the VM EM for both regions.

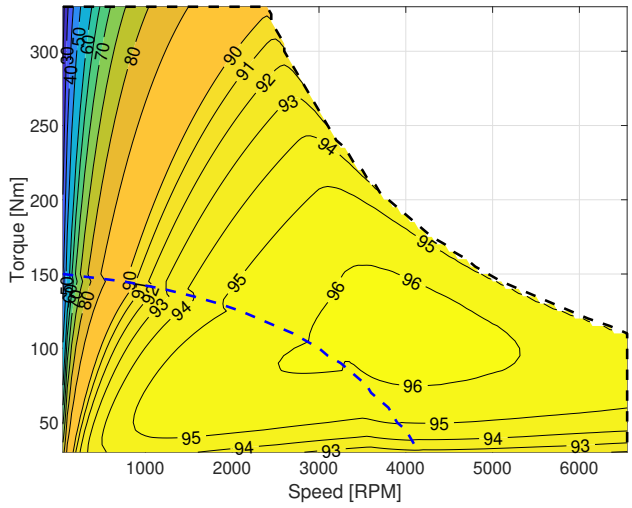

FIGURE 2: VIRGIN MAGNET EM EFFICIENCY MAP

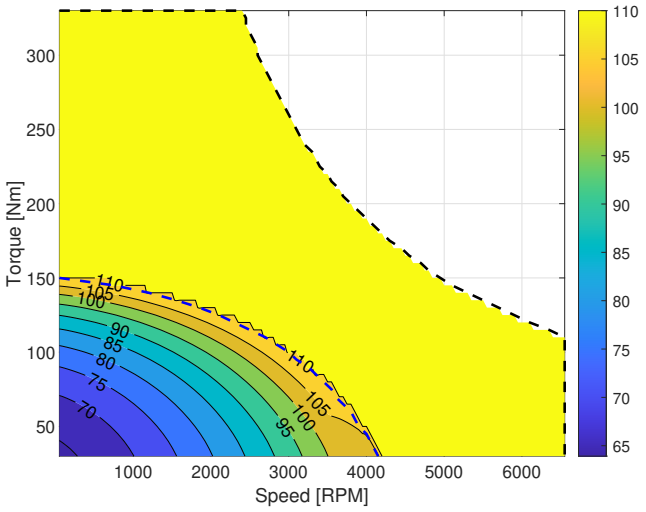

FIGURE 3: VIRGIN MAGNET EM TEMPERATURE MAP

Moreover, the plots also consider two control modes: the maximum torque per ampere (MTPA) and field-weakening (FW) mode. The MTPA mode is limited to a converter bus DC voltage of 345.6 V. The motor operates in FW mode when this voltage limit is reached. Both control modes are evident for the peak torque curve since this voltage limit is reached at the corner point. Operating points beyond the corner speed are within FW control mode. However, it is not evident for the S1 curve. So additionally, the performance comparison is presented for the S1 base operating point of 100 Nm at 2750 RPM with virgin and recycled magnets. The results can be seen in Tab. 2.

Figure 4 shows the efficiency map for the RM EM, and Fig. 5 shows the recycled magnet temperatures in both operating regions, continuous and peak. Results in Tab. 2 and the figures illustrated thus far show that although there is a slight performance

TABLE 1: RECYCLED MAGNET CHARACTERISATION DATA

Variable	T23	T80	T100	T119	T150	Average	Unit
Br	1.23	1.17	1.14	1.11	1.06	1.14	[T]
H_{cB}	938.6	816.3	692.1	562.9	405.3	683.1	[kA/m]
H_{cJ}	1439	899.6	740.2	587.9	416.6	816.6	[kA/m]
$(BH)_{max}$	291.7	256.6	241.6	224.5	195.1	241.9	[kJ/m^3]
B_a	0.62	0.59	0.58	0.56	0.59	0.59	[T]
H_a	471.5	433.5	417.9	400.4	331.1	410.9	[kA/m]
J_k	1.11	1.05	1.03	1.00	0.957	1.03	[T]
H_k	1328	806.6	653.6	521.7	361.3	734.2	[kA/m]
H_{max}	995.4	998.8	999.9	1000	999.4	998.7	[kA/m]
T	23.0	80.0	100	119	150	94.4	[°C]

TABLE 2: VIRGIN VS. RECYCLED MAGNET PERFORMANCE

Variable	Virgin	Recycled	Unit
Br @23°C	1.30	1.23	[T]
Br @100°C	1.18	1.14	[T]
Copper temperature	141.3	149.8	[°C]
Magnet temperature	106.4	109	[°C]
Speed	2750	2750	[RPM]
Mechanical torque	100	100	[Nm]
Efficiency	96.01	95.72	[%]
Input power	29995	30086	[W]
Power factor	0.928	0.917	[-]
Input line current	106.6	112.5	[A_{RMS}]

degradation, the RM EM performs similarly. In particular, the magnet temperature varies marginally within the continuous region. The efficiency change between the two machines can be highlighted, taking the difference of the two matrices representing the efficiency values for each torque-speed combination, as seen in Fig. 6. It can be noted that due to the shift of the efficiency regions of the RM EM map, the highest efficiency drop is below five percent for low speed and high torque values.

4. VEHICLE MODELLING

A LCV has been utilised for the purpose of quantifying the effects of magnet properties at system level. The vehicle is a HEV, with the powertrain characterised by a P2 configuration, meaning the EM is located after the clutch on the driveline as can be seen in Fig. 7. The machine is coaxial, thus no belt pulley is employed. The vehicle is simulated in MATLAB and Simulink® as a forward model due to its higher accuracy, with the inclusion of the driver modelled as a Proportional-Integral (PI) controller. This variant of modelling includes component limitations and their dynamics. On the other hand, a backward model does not incorporate the driver block and uses the reference speed from the driving cycle as the speed of the vehicle. This proves to be less computationally heavy, however falls short in accurately modelling the system. Furthermore, in order to control the energy distribution between the EM and the ICE of the vehicle, an Equivalent Consumption Minimisation Strategy (ECMS) is employed [20, 21]. It is a causal local optimisation method, whereby it aims to reduce the total equivalent energy

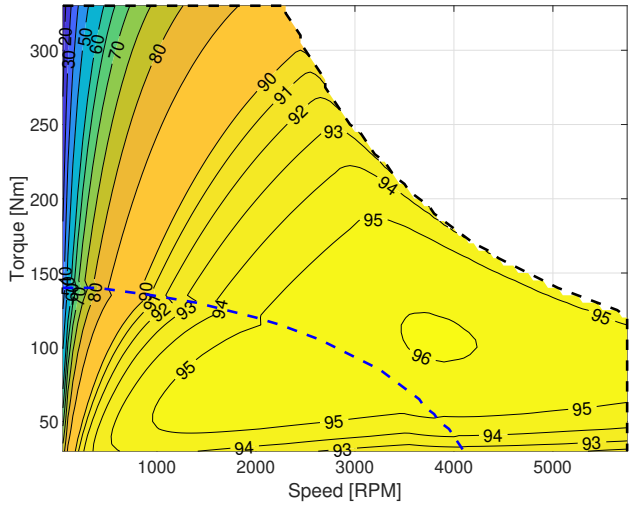

FIGURE 4: RECYCLED MAGNET EM EFFICIENCY MAP

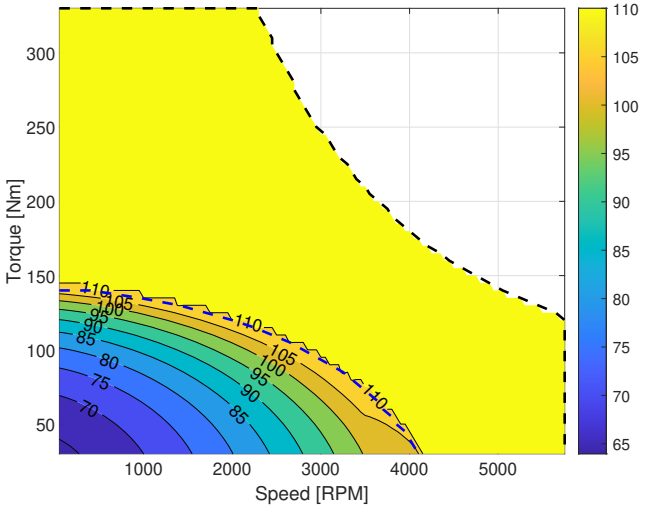

FIGURE 5: RECYCLED MAGNET EM TEMPERATURE MAP

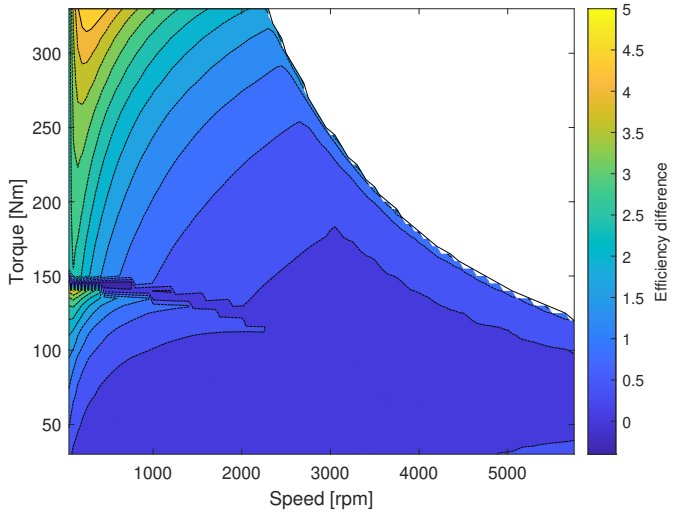

FIGURE 6: EFFICIENCY DEGRADATION

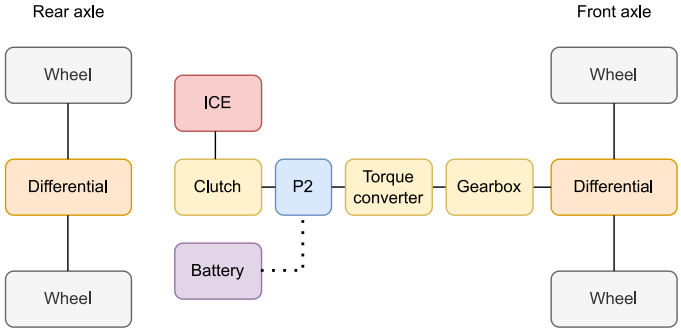

FIGURE 7: P2 ARCHITECTURE

consumption of the system through the consideration of certain boundaries. It is causal due to its dependency on multiple states of the vehicle, optimising the torque split on the basis of these values at each time instant of the drive cycle.

The working principle of the model is as follows: The driver block receives an error computed on the basis of the reference speed and the actual speed from the vehicle from which it generates a torque request. This request along with constraint parameters crucial for the ECMS algorithm are utilised by the controller to output an ICE and EM torque request. The sum of the two leads to the total torque required from the powertrain. This signal is delivered to the powertrain block which houses the torque converter, gearbox and differential blocks which take into account the respective efficiencies and parameters. In particular, the gear shifting strategy is in terms of the speed of the vehicle, dictating the choice of upshifiting or downshifting. The speed of the vehicle at which upshifting or downshifting is needed is given by:

$$v = \frac{n_{min/max} \cdot R_{wh} \cdot \pi}{U \cdot U_f \cdot 30} \tag{1}$$

where $n_{min/max}$ is the minimum or maximum rotational speed of the driveline, R_{wh} is the radius of the wheel, U is the current gear ratio and U_f is the final gear ratio. The vehicle block based on longitudinal dynamics computes the speed of the vehicle and sends this information to the driver, thus closing the system. The vehicle parameters are reported in Tab. 3, while Fig. 8 displays the logic described thus far.

TABLE 3: VEHICLE PARAMETERS

Parameters	Value	Unit
Mass	3100	[kg]
Drag coefficient	0.316	[-]
Frontal area	4.581	[m^2]
ICE characteristics	2.3 l/350 Nm peak	[-]
EM characteristics	PMSM 330 Nm peak	[-]
Battery nominal voltage	345.6	[V]
Battery capacity	20	[Ah]
Transmission	8-speed automatic	[-]
Final gear ratio	3.62	[-]
Wheel radius	0.35	[m]
Rolling resistance	0.01	[-]

The battery pack is modelled as an ideal voltage source in series with an internal resistance with no particular limitations, following the formulation:

$$V = V_0 \left(\frac{SOC}{1 - \beta(1 - SOC)} \right) \tag{2}$$

where V_0 is the nominal battery voltage, SOC is the state-of-charge and β is a characteristic parameter. The SOC is updated at each instant based on the power (whether it is outgoing or in-going) of the EM. More accurate estimations of the SOC have been proposed through the use of analytical [22] and data-driven models [23], with state-of-health (SOH) estimations included as well [24]. The model selected for this work has been merited to be sufficient to compute the SOC.

The ECMS algorithm employed follows the subsequent methodology: the ICE and EM maps are initialised offline such that they are called upon in the model as look-up tables (LUTs). They are present both in the controller and in the plant. The plant provides the SOC, maximum and minimum available torque values and the driveline speed (rotational speed is the same for the ICE and EM as no pulley is present) as feedback parameters. Furthermore, as seen in [25], the ECMS follows a set of constraints, summarised in the following:

$$\begin{cases} T_{req}(t) = T_{ICE}(t) + T_{EM}(t) \\ 0 \leqslant T_{ICE}(t) \leqslant T_{ICE}(\omega_{EM}) \\ T_{EM,min}(\omega_{EM}) \leqslant T_{EM}(t) \leqslant T_{EM,max}(\omega_{EM}) \\ SOC_{min} \leqslant SOC(t) \leqslant SOC_{max} \end{cases} \tag{3}$$

where T_{req} is the requested torque, T_{ICE} is the ICE torque and T_{EM} is the EM torque. $T_{EM,min}$ is the minimum available torque for generation, $T_{EM,max}$ is the maximum available torque for traction, SOC_{min} is the SOC lower bound and finally SOC_{max} is the SOC upper bound. The SOC must be kept within bounds in order to maintain an adequate battery health so as to not stress it

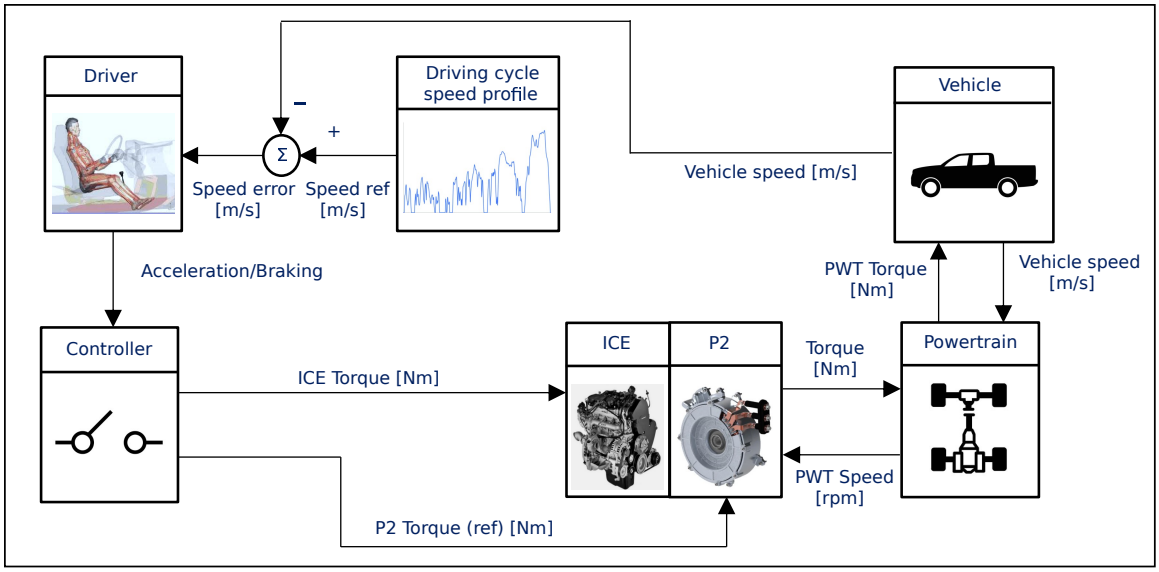

FIGURE 8: FORWARD P2 MODEL

with deep charging and discharging cycles. In this case study the bounds are limited to 20% for the lower and 90% for the upper. As will be evident in Section 5 of this work, the variation is mitigated with the controller action rather than the bounds. Following this, the algorithm produces a set of candidates of the control variable u defined as the ratio of the EM torque over the requested torque as seen in:

$$u(t) = \frac{T_{EM}(t)}{T_{req}(t)} \tag{4}$$

From this set of candidates the equivalent mass flow rate of the EM is computed through:

$$\dot{m}_{EM} = \frac{P_{EM}}{\eta_{EM} \cdot Q_f} \tag{5}$$

with P_{EM} being the power of the EM, η_{EM} the EM efficiency and Q_f the lower heating value of the fuel. A vector of mass flow rates is generated, along with a vector of mass flow rates for the ICE making use of the LUT. The efficiency of the EM is evaluated with the efficiency map as a LUT. The equivalent mass flow rate may be expressed as follows:

$$\dot{m}_{eq} = \dot{m}_{ICE} + s \cdot \dot{m}_{EM} \tag{6}$$

where s is the equivalence factor responsible for associating the virtual fuel consumption with the use of electrical energy and $\dot{m}_{ICE}$ is the ICE fuel mass flow rate. The factor is defined through the following formulation:

$$s(t) = s_{0,dis} + k_p(SOC_{ref} - SOC(t)) \tag{7}$$

where $s_{0,dis}$ is the constant discharge coefficient, k_p is a tunable parameter, SOC_{ref} is the reference SOC and SOC is the instantaneous SOC from the plant. The expression facilitates an adaptive evolution of the factor such that the SOC is properly maintained close to the reference value. In particular, as the vehicle under study is a HEV, the initial and final SOCs must be the same such that an accurate fuel consumption value may be evaluated. If the final SOC is greater than the reference/initial value, this implies the ICE has been utilised more to regenerate the portion of charge in excess. This would lead to a fuel consumption of the vehicle that is greater than it should be, creating misleading results.

With the minimisation of the equivalent mass flow rate, the optimal control variable may be selected and implemented into the following formulation to obtain the EM and ICE torque as a response to the requested torque from the driver:

$$\begin{cases} T_{ICE} = (1 - u(t)) \cdot T_{req} \\ T_{EM} = u(t) \cdot T_{req} \end{cases} \tag{8}$$

The model is tuned such that the charge sustaining (CS) condition is met. The ECMS is maintained constant between the two cases: VM EM and RM EM, as the variation of the SOC between the two is not significant enough to merit the modification of the equivalence factor. This will be examined in the following section.

5. RESULTS AND DISCUSSION

With the EM and vehicle modelled, the former is implemented into the latter to assess the effect the recycled magnets have on the HEV performance. The unloaded vehicle is evaluated on the official homologation driving cycle, the World Harmonized Light Vehicle Test Procedure (WLTP). The baseline vehicle includes the VM EM, while the vehicle under test includes the RM EM. With a slight degradation seen at component level, the vehicle performance decrease is seen to be insignificant. This can be outlined in Tab. 4, where the vehicle incurs only a 0.01 [L/100km] increase with respect to the baseline vehicle.

Regarding the state-of-charge over the driving cycle in Fig. 9, it can be noticed that the two cases behave in an almost

TABLE 4: PERFORMANCE COMPARISON UNLOADED

Parameters	VM EM	RM EM	Difference
Fuel [L/100km]	9.05	9.06	0.01
CO_2 [gCO_2/km]	238.9	239.2	0.3

TABLE 5: ENERGY COMPARISON UNLOADED

Parameters	VM EM	RM EM
Motoring		
Electrical Energy [kJ]	4493	4473
Mechanical Energy [kJ]	4289	4261
Generating		
Electrical Energy [kJ]	-4505	-4478
Mechanical Energy [kJ]	-4818	-4818

identical manner. Due to the evidently minor variation of the final SOC between the VM EM and the RM EM seen in Fig. 10, the ECMS is not tuned for the latter case as stated previously. In some instances one may observe lower discharge of the battery, an indication of a small number of operating points that are not selected in the RM EM case due to the degradation of efficiency. This translates to a minor increase in fuel consumption, where Fig. 11 indicates the consumption over the drive cycle and Fig. 12 exhibits the fuel economy decrease. The SOC for the RM EM reaches a final value just under that of the VM EM, suggesting the presence of operating points with lower efficiencies that incur higher power consumption from the battery. This can be reasonably stated given the operating points for the two cases are similar. These comments can also be extended towards the regeneration, where the lower RM EM efficiency translates to a slightly lower recovery of braking energy, and thus the final SOC is lower. Table 5 displays the electrical and mechanical energies for the systems with the respective EMs and supports the claims made thus far. The mechanical energy represents the energy requested from the EM, while the electrical energy is that which considers the efficiency of the EM. The RM EM case indicates a minor decrease in regenerated electrical energy, as well as a lower mechanical energy indicating a lower employment of the EM during operation. It can be noted that the overall performance degradation is around 0.11%, suggesting an extremely similar behaviour between the VM EM and RM EM at vehicle level.

To understand the performance similarity at vehicle level more thoroughly, select operating points of the RM EM across the drive cycle are plotted on the efficiency degradation map as seen in Fig. 13. The black points correspond to the homologation procedure, where the vehicle is unloaded. The red points correspond to the vehicle with a payload of 1.9 t, leading to a gross mass of 5 t. Considering the positive quadrant, it is evident that a number of operating conditions in the unloaded case fall into regions that exhibit between 0% and 0.5% of degradation for the RM EM. For the loaded case, the RM EM is employed for

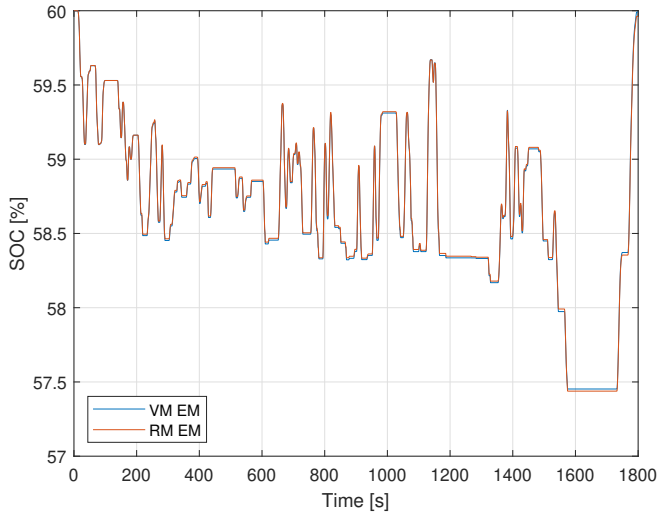

FIGURE 9: BATTERY SOC COMPARISON WITH RM AND VM EM

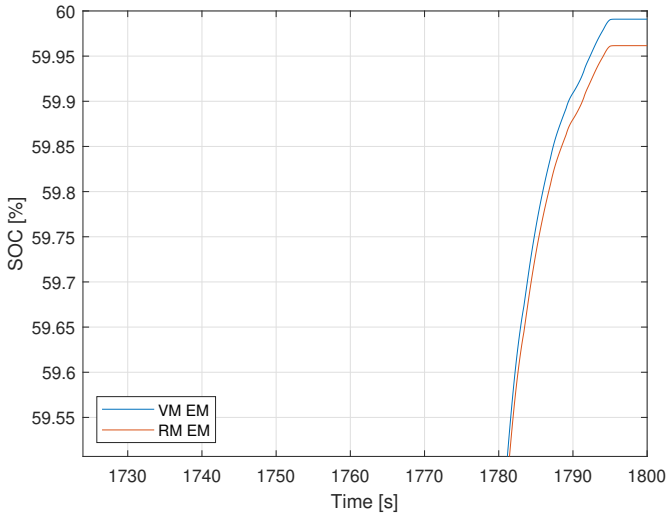

FIGURE 10: ENLARGED PORTION OF SOC COMPARISON WITH RM AND VM EM

greater torque values due to the increased mass of the vehicle. The constant discharge coefficient in the equivalence factor is increased both for the VM EM and RM EM loaded cases to ensure balancing of the SOC across the driving cycle. The RM EM ECMS coefficient is increased by 19% with respect to the unloaded case, while the VM EM ECMS coefficient is increased by 9%. This subsequently decreases the usage of the RM EM compared to the VM EM and incurs a lower fuel economy. The degradation of efficiency of the system in the loaded case is around 1.2%, with the relevant performance parameters collected in Tab. 6. Table 7 provides the electrical and mechanical energies over the drive cycle for the loaded case. In this case, the RM EM is seen to be regenerating a lower portion of the recoverable energy, while also providing less energy for propulsion.

Figure 14 displays the operating points of the RM EM during

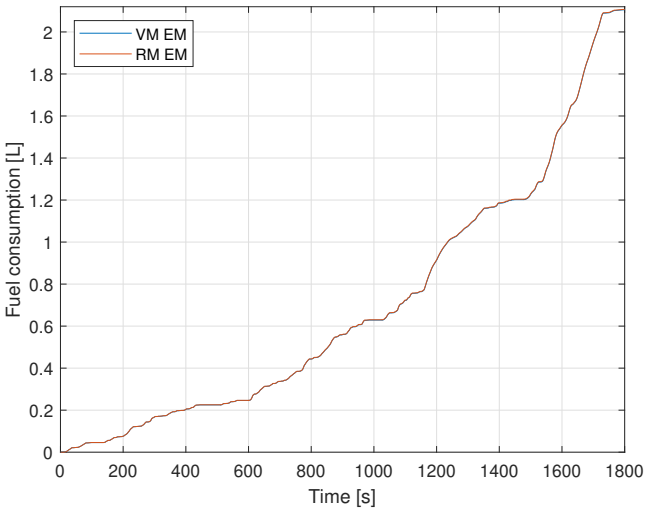

FIGURE 11: VEHICLE FUEL CONSUMPTION COMPARISON WITH RM AND VM EM

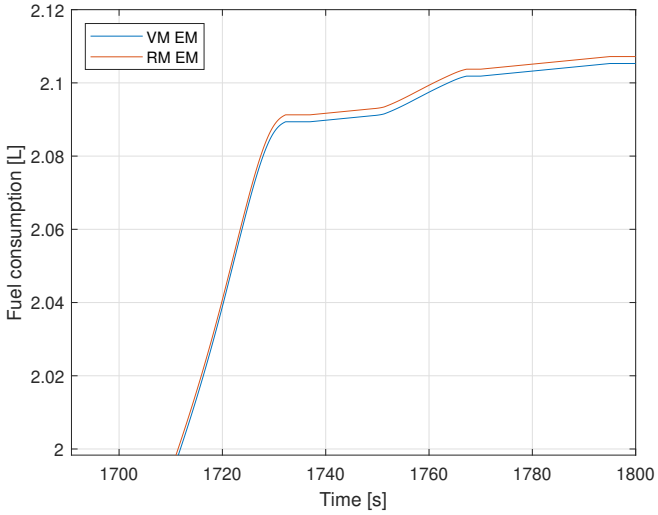

FIGURE 12: ENLARGED PORTION OF FUEL CONSUMPTION COMPARISON WITH RM AND VM EM

regeneration for the unloaded and loaded cases. It is evident that almost the full regenerating potential is utilised regarding the unloaded case, while the full regenerative capability is exploited in the loaded case. This can be attributed to a higher mass regarding the latter, where there is a larger amount of braking potential energy present. The regenerative behaviour is due to the ECMS algorithm, where the efficiency is taken into account only in motoring mode, and the EM is free to recover as much braking energy as it can when the torque request is negative. This can also be noted as a great advantage of employing a P2 architecture, where the clutch disengages from the ICE during braking so as to maximize energy recovery. In addition, it may be noticed where the minimum rotational speed is set by considering the regeneration operating points. As the vehicle is braking, the gear shifting strategy downshifts when the minimum rotational speed

TABLE 6: PERFORMANCE COMPARISON LOADED

Parameters	VM EM	RM EM	Difference
Fuel [L/100km]	11.49	11.63	0.14
CO_2 [gCO_2/km]	303.3	307.0	3.7

TABLE 7: ENERGY COMPARISON LOADED

Parameters	VM EM	RM EM
Motoring		
Electrical Energy [kJ]	7604	7450
Mechanical Energy [kJ]	7230	7112
Generating		
Electrical Energy [kJ]	-7637	-7531
Mechanical Energy [kJ]	-8387	-8387

is reached, thus increasing the driveline speed until it reaches this threshold again. This process continues until the vehicle reaches a stop or is requested to accelerate aiming to follow the driving cycle.

6. CONCLUSIONS

The work presented has the intention to study the effect recycled magnets have on EM and vehicle performances. With the characterisation of the magnets performed and the EM modelled, it has been shown that there is a low degradation at component level and subsequently a low decrease in performance at vehicle level. The loaded LCV case indicates a higher fuel consumption for the RM EM due to the vehicle's larger mass, mainly as a consequence of the higher equivalence factor in the ECMS compared to that of the VM EM. It may be concluded that the use of recycled magnets in EMs for automotive applications does not hinder vehicle performance to a large extent, and would offer economic and environmental benefits if implemented. In addition, experimental validation of the numerical results presented must be performed, entailing the testing of the VM EM and RM EM in static and dynamic conditions.

ACKNOWLEDGMENTS

The authors would like to thank the European Institute of Technology (EIT) for its support in funding the eMotor Virtual Test Bed (e-VTB) project, from which this work has been developed. In addition, the authors would like to thank Matej Zaplotnik for his contribution to the project in providing data as well as Dayco Europe and Ningbo Physis Technology for their close collaboration. Finally, the authors acknowledge gratefully the role Santer Reply and Concept Reply took as project coordinators.

REFERENCES

[1] "CO_2 emission performance standards for cars and vans." Accessed 2023-03-03, URL https://climate.ec.europa.eu/eu-action/transport-emissions/road-transport-reducing-co2-emissions-vehicles/co2-emission-performance-standards-cars-and-vans_en.

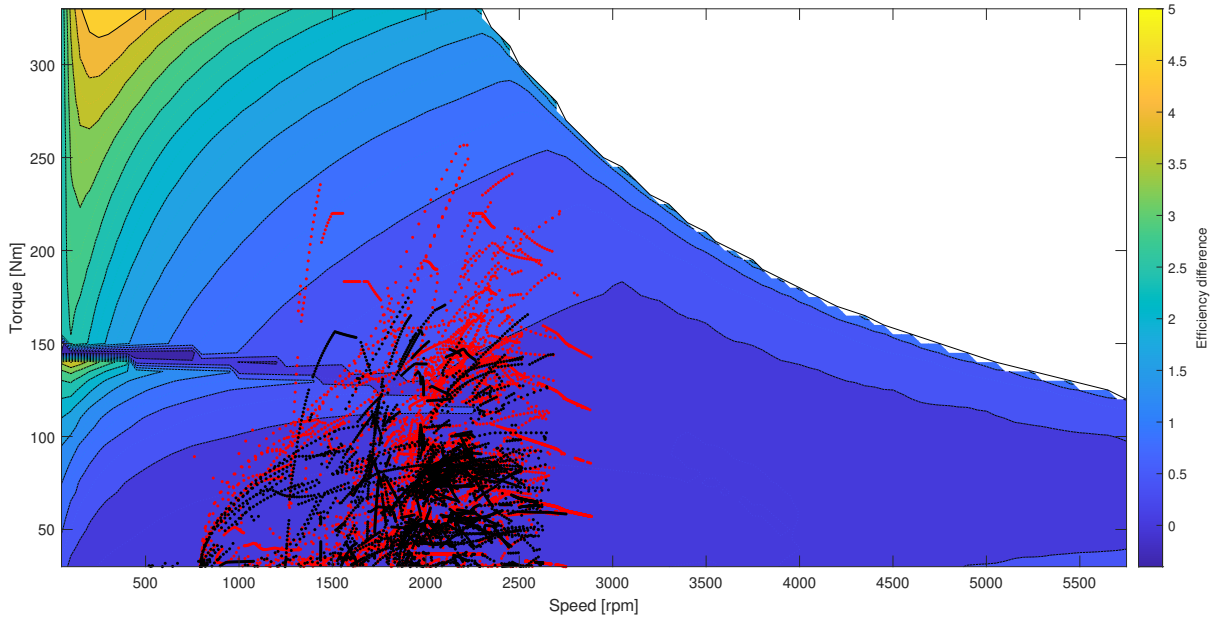

FIGURE 13: EFFICIENCY DEGRADATION AND OPERATING POINTS OF THE RM EM IN MOTORING MODE

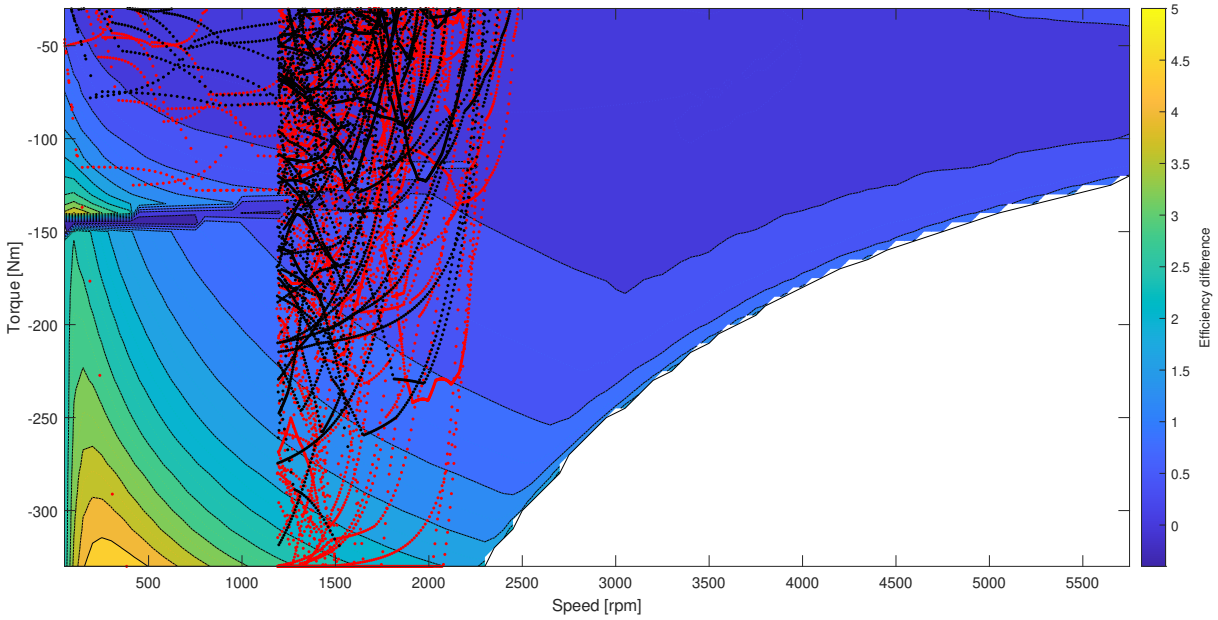

FIGURE 14: EFFICIENCY DEGRADATION AND OPERATING POINTS OF THE RM EM IN GENERATING MODE

[2] Mohr, Steve H., Mudd, Gavin M. and Giurco, Damien. "Lithium Resources and Production: Critical Assessment and Global Projections." *Minerals* Vol. 2 No. 1 (2012): pp. 65–84. DOI 10.3390/min2010065.

[3] Dushyantha, Nimila, Batapola, Nadeera, Ilankoon, I.M.S.K., Rohitha, Sudath, Premasiri, Ranjith, Abeysinghe, Bandara, Ratnayake, Nalin and Dissanayake, Kithsiri. "The story of rare earth elements (REEs): Occurrences, global distribution, genesis, geology, mineralogy and global production." *Ore Geology Reviews* Vol. 122 (2020): p. 103521. DOI 10.1016/j.oregeorev.2020.103521.

[4] Pražanová, Anna, Knap, Vaclav and Stroe, Daniel-Ioan. "Literature Review, Recycling of Lithium-Ion Batteries from Electric Vehicles, Part II: Environmental and Economic Perspective." *Energies* Vol. 15 No. 19 (2022): p. 7356. DOI 10.3390/en15197356.

[5] Yang, Yongxiang, Walton, Allan, Sheridan, Richard, Güth, Konrad, Gauß, Roland, Gutfleisch, Oliver, Buchert, Matthias, Steenari, Britt-Marie, Van Gerven, Tom, Jones, Peter Tom and Binnemans, Koen. "REE Recovery from End-of-Life NdFeB Permanent Magnet Scrap: A Critical Review." *Journal of Sustainable Metallurgy* Vol. 3 No. 1 (2017): pp. 122–149. DOI 10.1007/s40831-016-0090-4.

[6] Jönsson, Christian, Awais, Muhammad, Pickering, Lydia, Degri, Malik, Zhou, Wei, Bradshaw, Andy, Sheridan, Richard, Mann, Vicky and Walton, Allan. "The extraction of NdFeB magnets from automotive scrap rotors using hydrogen." *Journal of Cleaner Production* Vol. 277 (2020): p. 124058. DOI 10.1016/j.jclepro.2020.124058.

[7] Li, Ziwei, Kedous-Lebouc, Afef, Dubus, Jean-Marc, Garbuio, Lauric and Personnaz, Sophie. "Direct reuse strategies of rare earth permanent magnets for PM electrical machines – an overview study." *The European Physical Journal Applied Physics* Vol. 86 No. 2 (2019): p. 20901. DOI 10.1051/epjap/2019180289.

[8] Sprecher, Benjamin, Xiao, Yanping, Walton, Allan, Speight, John, Harris, Rex, Kleijn, Rene, Visser, Geert and Kramer, Gert Jan. "Life Cycle Inventory of the Production of Rare Earths and the Subsequent Production of NdFeB Rare Earth Permanent Magnets." *Environmental Science & Technology* Vol. 48 No. 7 (2014): pp. 3951–3958. DOI 10.1021/es404596q.

[9] Onori, Simona, Serrao, Lorenzo and Rizzoni, Giorgio. *Hybrid Electric Vehicles*. SpringerBriefs in Electrical and Computer Engineering, Springer London, London (2016). DOI 10.1007/978-1-4471-6781-5.

[10] Jin, Hongyue, Afiuny, Peter, McIntyre, Timothy, Yih, Yuehwern and Sutherland, John W. "Comparative Life Cycle Assessment of NdFeB Magnets: Virgin Production versus Magnet-to-Magnet Recycling." *Procedia CIRP* Vol. 48 (2016): pp. 45–50. DOI 10.1016/j.procir.2016.03.013.

[11] Prosperi, D., Bevan, A.I., Ugalde, G., Tudor, C.O., Furlan, G., Dove, S., Lucia, P. and Zakotnik, M. "Performance comparison of motors fitted with magnet-to-magnet recycled or conventionally manufactured sintered NdFeB." *Journal of Magnetism and Magnetic Materials* Vol. 460 (2018): pp. 448–453. DOI 10.1016/j.jmmm.2018.04.034.

[12] Reck, Barbara K. and Graedel, T. E. "Challenges in Metal Recycling." *Science* Vol. 337 No. 6095 (2012): pp. 690–695. DOI 10.1126/science.1217501.

[13] Habib, Komal and Wenzel, Henrik. "Exploring rare earths supply constraints for the emerging clean energy technologies and the role of recycling." *Journal of Cleaner Production* Vol. 84 (2014): pp. 348–359. DOI 10.1016/j.jclepro.2014.04.035.

[14] Schueler, Doris, Buchert, Matthias, Liu, Ran, Dittrich, Stefanie and Merz, Cornelia. "Study on rare earths and their recycling. Final report." (2011).

[15] Proelss, Juliane, Schweizer, Denis and Seiler, Volker. "The economic importance of rare earth elements volatility forecasts." *International Review of Financial Analysis* Vol. 71 (2020): p. 101316. DOI 10.1016/j.irfa.2019.01.010.

[16] "European Training Network for the Design and Recycling of Rare-Earth Permanent Magnet Motors and Generators in Hybrid and Full Electric Vehicles (DEMETER)." Accessed 2023-03-03, URL https://etn-demeter.eu/.

[17] "innovative RE-use and reCycling VALue Chain for High-Power Magnets." Accessed 2023-03-03, URL https://anr.fr/Project-ANR-13-RMNP-0013/.

[18] Walton, A., Yi, Han, Rowson, N.A., Speight, J.D., Mann, V.S.J., Sheridan, R.S., Bradshaw, A., Harris, I.R. and Williams, A.J. "The use of hydrogen to separate and recycle neodymium–iron–boron-type magnets from electronic waste." *Journal of Cleaner Production* Vol. 104 (2015): pp. 236–241. DOI 10.1016/j.jclepro.2015.05.033.

[19] Meakin, J.P., Speight, J.D., Sheridan, R.S., Bradshaw, A., Harris, I.R., Williams, A.J. and Walton, A. "3-D laser confocal microscopy study of the oxidation of NdFeB magnets in atmospheric conditions." *Applied Surface Science* Vol. 378 (2016): pp. 540–544. DOI 10.1016/j.apsusc.2016.03.182.

[20] Hegde, Shailesh, Bonfitto, Angelo, Galluzzi, Renato, Molina, Luis M. Castellanos, Amati, Nicola and Tonoli, Andrea. "Equivalent Consumption Minimization Strategy Based on Belt Drive System Characteristic Maps for P0 Hybrid Electric Vehicles." *Energies* Vol. 16 No. 1 (2023): p. 487. DOI 10.3390/en16010487.

[21] Rahmeh, Hadi, Bonfitto, Angelo and Ruzimov, Sanjarbek. "Fuzzy Logic vs Equivalent Consumption Minimization Strategy for Energy Management in P2 Hybrid Electric Vehicles." *Volume 4: 22nd International Conference on Advanced Vehicle Technologies (AVT)*: p. V004T04A026. 2020. American Society of Mechanical Engineers, Virtual, Online. DOI 10.1115/DETC2020-22431.

[22] Saldaña, Gaizka, San Martín, José Ignacio, Zamora, Inmaculada, Asensio, Francisco Javier and Oñederra, Oier. "Analysis of the Current Electric Battery Models for Electric Vehicle Simulation." *Energies* Vol. 12 No. 14 (2019): p. 2750. DOI 10.3390/en12142750.

[23] Feraco, Stefano, Anselma, Pier Giuseppe, Bonfitto, Angelo and Kollmeyer, Phillip J. "Robust Data-Driven Battery State of Charge Estimation for Hybrid Electric Vehicles." *SAE International Journal of Electrified Vehicles* Vol. 11 No. 2 (2021): pp. 213–230. DOI 10.4271/14-11-02-0017.

[24] Anselma, Pier Giuseppe, Kollmeyer, Phillip J., Feraco, Stefano, Bonfitto, Angelo, Belingardi, Giovanni, Emadi, Ali, Amati, Nicola and Tonoli, Andrea. "Assessing Impact of Heavily Aged Batteries on Hybrid Electric Vehicle Fuel Economy and Drivability." *2021 IEEE Transportation Electrification Conference & Expo (ITEC)*: pp. 696–701. 2021. IEEE, Chicago, IL, USA. DOI 10.1109/ITEC51675.2021.9490149.

[25] Hegde, Shailesh, Bonfitto, Angelo, Rahmeh, Hadi, Amati, Nicola and Tonoli, Andrea. "Optimal Selection of Equivalence Factors for ECMS in Mild Hybrid Electric Vehicles." *Volume 1: 23rd International Conference on Advanced Vehicle Technologies (AVT)*: p. V001T01A019. 2021. American Society of Mechanical Engineers, Virtual, Online. DOI 10.1115/DETC2021-71621.